Inorganic Chemistry
Article

Inorg. Chem. **2010**, *49*, 10557–10570 **10557**
DOI: 10.1021/ic101447q

Spectroscopic and Magnetic Properties of a Series of μ-Cyano Bridged Bimetallic Compounds of the Type $M^{II}-NC-Fe^{III}$ (M = Mn, Co, and Zn) Using the Building Block $[Fe^{III}(CN)_5imidazole]^{2-}$

Heloïse Tchouka,[†] Auke Meetsma,[‡] and Wesley R. Browne*,[†,‡]

[†]*Stratingh Institute for Chemistry, University of Groningen, Nijenborgh 4, 9747 AG Groningen, The Netherlands, and* [‡]*Zernike Institute for Advanced Materials, University of Groningen, Nijenborgh 4, 9747 AG Groningen, The Netherlands*

Received July 20, 2010

In this contribution, we describe the preparation and single-crystal X-ray diffraction of a new building block for bimetallic solid state materials. X-ray diffraction data of these complexes indicate that $(PPh_4)_2[Fe(CN)_5imidazole]\cdot 2H_2O$ crystallizes in the triclinic space group $P\bar{1}$ with a = 9.8108(15) Å, b = 11.1655(17) Å, c = 23.848(4) Å, α = 87.219(2)°, β = 85.573(2)°, γ = 70.729(2)°, and Z = 2, while its precursor $Na_3[Fe(CN)_5(en)]\cdot 5H_2O$ crystallizes in the monoclinic space group $P2_1/n$ with a = 8.3607(7) Å, b = 11.1624(9) Å, c = 17.4233(14) Å, β = 90.1293(9)°, and Z = 4. Spectroscopic and magnetic properties of a series of bimetallic materials were obtained by reaction of the complex $[Fe(CN)_5imidazole]^{2-}$ with hydrated transition metal ions $[M(H_2O)_n]^{2+}$ (M = Mn, Co, Zn; n = 4 or 6). The new bimetallic materials obtained are $[Co(H_2O)_2][Fe(CN)_5imidazole]\cdot 2H_2O$ (**1**), $[Mn(CH_3OH)_2][Fe(CN)_5imidazole]$ (**2**), $Zn[Fe(CN)_5imidazole]\cdot H_2O$ (**3**), and $[Mn(bpy)][Fe(CN)_5imidazole].H_2O$ (**4**). All of the complexes crystallize in the orthorhombic system. X-ray single-crystal analysis of the compounds identified the *Imma* space group with a = 7.3558(10) Å, b = 14.627(2) Å, c = 14.909(2) Å, and Z = 4 for **1**; the $P2_12_12_1$ space group with a = 7.385(5) Å, b = 13.767(9) Å, c = 14.895(10) Å, and Z = 4 for **2**; the *Pnma* space group with a = 13.783(2) Å, b = 7.167(11) Å, c = 12.599(2) Å, and Z = 4 for **3**; and the *Pnma* space group with a = 13.192(3) Å, b = 7.224(16) Å, c = 22.294(5) Å, and Z = 4 for **4**. The structures of **1**, **2**, and **4** consist of two-dimensional network layers containing, as the repeating unit, a cyclic tetramer $[M_2Fe_2(CN)_4]$ (M = Mn, Co). H bonding between the layers in the structure of **1** results in a quasi-three-dimensional network. The structure of **3** was found to be three-dimensional, where all of the cyano ligands are involved in bridging between the metal centers. The bridging character of the cyano is confirmed spectroscopically. The magnetic properties have been investigated for all of the bimetallic systems. Compound **1** shows ferromagnetic behavior with an ordering temperature at 25 K, which is higher than the corresponding Prussian Blue analogue $Co_x[Fe(CN)_6]_y\cdot zH_2O$. Compound **2** shows weak ferromagnetic behavior and an interlayer antiferromagnetic character, while **3**, as expected, shows paramagnetic character due to the diamagnetic character of Zn^{2+}. Compound **4** shows antiferromagnetic behavior.

Introduction

Strong σ-donor properties and the ability to coordinate via the C or N atom or both have placed the CN^- ligand centrally in the preparation of ligand-bridged multimetallic complexes. This is especially the case for Prussian Blue analogues where the mixing of a hydrated transition metal ion, e.g., $[M(H_2O)]^{m+}$, with hexacyanoferrate ions $[Fe(CN)_6]^{n-}$ has provided bimetallic compounds of the type $M_x[Fe(CN)_6]_y\cdot zH_2O$ (where M is a transition metal), the so-called Prussian Blue analogs.[1] Importantly, the short internuclear separation provided for by the CN^- ligand allows for such bimetallic systems to exhibit magnetic and optical properties not observed in the individual components. Bimetallic complexes in particular are of special interest for their electro- and opto-magnetic[2] properties because of their potential application in information storage and quantum computing. However, the study of such systems has been hampered by the insolubility of such compounds and the difficulty encountered in obtaining single-crystalline materials suitable for X-ray structure determination.

---

*To whom correspondence should be requested. E-mail: w.r.browne@rug.nl.

(1) (a) Mallah, T.; Thiébaut, S.; Verdaguer, M.; Veillet, P. *Science* **1993**, *262*, 1544. (b) Entley, R. W.; Girolami, G. S. *Inorg. Chem.* **1994**, *33*, 5165. (c) Ferlay, S.; Mallah, T.; Ouahès, R.; Veillet, P.; Verdaguer, M. *Nature* **1995**, *378*, 701. (d) Entley, R. W.; Girolami, G. S. *Science* **1995**, *268*, 397. (e) Buschmann, W. E.; Paulson, S. C.; Wynn, C. M.; Girtu, M.; Epstein, A. J.; White, H. S.; Miller, J. S. *Chem. Mater.* **1998**, *10*, 1386. (f) Verdaguer, M.; Bleuzen, A.; Marvaud, V.; Vaissermann, J.; Seuleiman, M.; Desplanches, C.; Scuiller, A.; Train, C.; Garde, R.; Gelly, G.; Lomenech, C.; Rosenman, I.; Veillet, P.; Cartier, C.; Villain, F. *Coord. Chem. Rev.* **1999**, *190−192*, 1023. (g) Holmes, S. M.; Girolami, G. *J. Am. Chem. Soc.* **1999**, *121*, 5593. (h) Halevik, Ø.; Buschmann, W. E.; Zhang, J.; Manson, J.; Miller, J. S. *Adv. Mater.* **1999**, *11*, 914.

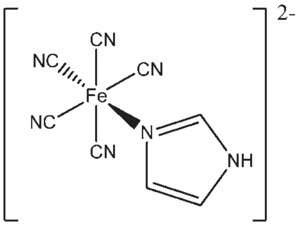

Figure 1. Molecular structure of the $[Fe(CN)_5imidazole]^{2-}$ building block.

The physical behavior of the Prussian Blue analogs was shown to be influenced by the degree of defects in their structure. These defects can be controlled by the proportion and/or type of alkali cation employed[3,4] during preparation.[5] The $[Fe(CN)_6]^{3-}$ paradigm can also be extended through the use of a substituted cyanoferrate complex[6] as a building block. In addition to tuning the molecular properties, this also results in changes to the structural properties of the bimetallic material formed. The dimensionality of these bimetallic systems can be tuned further by adding a multidentate ligand to the system.[7,8] To date, the substituted pentacyano ferrate complex of the type $[Fe(CN)_5L]^{n-}$ that has seen most widespread use is sodium nitroprusside ($[Fe(CN)_5NO]^{2-}$), not least because the photoirradiation[9] of this anion has been shown to enhance the magnetization of the nickel nitroprusside complex ($Ni[Fe(CN)_5NO]\cdot 5.3H_2O$).[10]

The complex $Li_2[Fe^{III}(CN)_5imidazole]$, in which the Fe(III) ion is coordinated by five cyano ligands and one of the nitrogen atoms of the imidazole ligand, is potentially an alternative to nitroprusside. In this report, the $[Fe(CN)_5imidazole]^{2-}$ ion (Figure 1) is employed as a building block in the preparation of a new series of bimetallic compounds in which the cyano ligands form bridges between the metal centers. The presence of the imidazole ligand in the structure can influence the bimetallic compounds formed in terms of their general properties compared to the corresponding Prussian Blue analogs.

The new cyanide-bridged bimetallic materials of the type $M^{II}[Fe^{III}(CN)_5imidazole]\cdot xH_2O$ (M = Mn, Co, and Zn) formed are characterized by single-crystal X-ray diffraction, vibrational and electronic spectroscopy, and magnetic methods. This series of compounds provides detailed information on the structure of such bimetallic systems and allows for correlations between structure, magnetic, and spectroscopic properties to be drawn.

Experimental Section

Material. Chemicals were used as received unless stated otherwise. $Li_2[Fe(CN)_5imidazole]\cdot 5H_2O$ was prepared by metathesis of $(PPh_4)_2[Fe(CN)_5imidazole]\cdot 2H_2O$ with $LiClO_4$ in acetonitrile.

Caution! *Perchlorate salts are potentially explosive. Only small quantities should be prepared and must be handled with suitable protective safeguards.*

Caution! *Sources of HCN should be treated with care and used in small quantities. Contact with acids should be avoided.*

$Na_3[Fe(CN)_5(en)]\cdot 5H_2O$. $Na_3[Fe(CN)_5(en)]\cdot 5H_2O$ was prepared by modification of the method of Olabe and Ayamonino:[11] $Na_2[Fe(CN)_5NO]\cdot 2H_2O$ (6 mmol, 2 g) and sodium acetate (12 mmol, 1 g) were dissolved in a mixture of water (20 mL) and ethanol (15 mL). After 30 min, an excess of ethylenediamine (10 mL) was added to the solution, and the solution was heated between 40 and 60 °C with stirring. After 30 min, an excess of ethanol (15 mL) was added to the solution. The solution was filtered hot and allowed to cool to room temperature. Yellow crystals of $Na_3[Fe(CN)_5(en)]\cdot 5H_2O$ were obtained following slow evaporation at room temperature and were collected by filtration. Yield: 86% (2.35 g). Anal. Calcd for $FeC_7N_7Na_3H_{18}O_5Na_3[Fe(CN)_5(en)]\cdot 5H_2O$: C, 20.76; H, 4.48; N, 24.20. Found: C, 20.97; H, 4.56; N, 23.79%.

$(PPh_4)_2[Fe(CN)_5(im)]\cdot 2H_2O$. Air was bubbled for 30 min through an aqueous solution (20 mL) of $Na_3[Fe(CN)_5C_2H_8N_2]\cdot 5H_2O$ (1.2 mmol, 1 g). Over 2 h, a color change from yellow to orange was observed. The solution was added slowly to a stirred solution (50 mL 3:2 water/ethanol) of tetraphenylphosphonium chloride (2.4 mmol). Red brownish crystals of $(PPh_4)_2[Fe(CN)_5(im)]\cdot 2H_2O$ formed upon standing (56%, 1.35 g). Anal. Calcd for $FeC_{56}P_2H_{48}N_7O_2$: C, 69.43; H, 4.99; N, 10.12. Found: C, 69.52; H, 4.88; N, 10.08%.

Preparation of Bimetallic Materials. $Co(H_2O)_2[Fe(CN)_5imidazole]\cdot 2H_2O$ (1). Compound **1** was obtained by slow diffusion between two test tubes (a small test tube placed within a larger test tube) of an aqueous solution of the $Li_2[Fe(CN)_5imidazole]$ (100 mg) in the inner test tube and an aqueous solution of $CoCl_2\cdot 6H_2O$ (100 mg) in the larger test tube. The solution was heated at 42 °C and allowed to stand in the dark. Dark red block crystals of **1** were collected after two weeks (yield 30 mg). Anal. Calcd for $C_8H_8CoFeN_7O_2\cdot 2H_2O$ (**1**): C, 24.96; H, 3.14; N, 25.47. Found: C, 25.61; H, 2.85; N, 25.52. Desolvated samples were prepared by heating 10 mg at 90 °C for 18 h under vacuum conditions. The mass loss (10−15%) is consistent with the loss of the water of crystallization.

$Mn(CH_3OH)_2[Fe(CN)_5imidazole]$ (2). The preparation of complex **2** was carried out using a procedure similar to that used for **1**. A total of 2 mL of an aqueous solution of $Mn(NO_3)_2\cdot 4H_2O$ (100 mg) and 2 mL of an aqueous solution of $Li_2[Fe(CN)_5imidazole]$ (100 mg) were each gently layered on opposite sides of an H tube initially filled with 12 mL of methanol. The solution was maintained at 42 °C. Dark red crystals of **2** were collected after two weeks (yield 97 mg). Anal. Calcd for $C_{10}H_{12}MnFeN_7O_2$ (**2**): C, 32.20; H, 3.24; N, 26.28. Found: C, 31.95; H, 2.88; N, 26.42.

$Zn[Fe(CN)_5imidazole]\cdot H_2O$ (3). The preparation of **3** was carried out as described for **1** except that $ZnCl_2\cdot 6H_2O$ (100 mg) was used in place of $CoCl_2\cdot 6H_2O$. Dark red (**3**) crystals were collected after one week (yield: 110 mg). Anal. Calcd for

---

(2) (a) Sato, O.; Iyoda, T.; Fujishima, A.; Hashimoto, K. *Science* **1996**, *271*, 49. (b) Ohkoshi, S.-I.; Fujishima, A.; Hashimoto, K. *J. Am. Chem. Soc.* **1998**, *120*, 5349. (c) Sato, O.; Iyoda, T.; Fujishima, A.; Hashimoto, K. *Science* **1996**, *271*, 704. (d) Sato, O.; Einaga, T.; Fujishima, A.; Hashimoto, K. *Inorg. Chem.* **1999**, *38*, 4405. (e) Sato, O.; Einaga, T.; Fujishima, A.; Hashimoto, K. *Inorg. Chem.* **1999**, *38*, 4405. (f) Mizno, M.; Ohkoshi, S.-I.; Hashimoto, K. *Adv. Mater.* **2000**, *12*, 1955.

(3) Bleuzen, A.; Lomenech, C.; Escax, V.; Villain, F.; Varret, F.; Cartier dit Moulin, C.; Verdarguer, M. *J. Am. Chem. Soc.* **2000**, *122*, 6648.

(4) Escax, V.; Bleuzen, A.; Cartier dit Moulin, C.; Villain, A. G.; Varret, F.; Verdaguer, M. *J. Am. Chem. Soc.* **2001**, *123*, 12536.

(5) Vertelman, E. J. M.; Maccalini, E.; Gournis, D.; Rudolf, P.; Bakas, T.; Luzon, J.; Broer, R.; Pugzlyz, A.; Lummen, T. T. A.; van Loosdrecht, P. H. M.; van Koningsbruggen, P. J. *Chem. Mater.* **2006**, *18*, 1951.

(6) Garg, A. N.; Goel, P. S. *Inorg. Chem.* **1971**, *10*, 1344.

(7) Fukita, N.; Ohba, M.; Okawa, H.; Matsuda, K.; Iwamura, H. *Inorg. Chem.* **1998**, *37*, 842.

(8) Berlinguette, C. P.; Dragulescu-Andrasi, A.; Sieber, A.; Galán-Mascarós, J. R.; Güdel, H. U.; Achim, C.; Dunbar, K. R. *J. Am. Chem. Soc.* **2004**, *126*, 6222.

(9) Woike, Th.; Krasser, W.; Bechthold, P. S.; Haussühl, S. *Phys. Rev. Lett.* **1984**, *53*, 73.

(10) (a) Gu, Z. Z.; Sato, O.; Iyoda, T.; Hashimoto, K.; Fujishima, A. *J. Phys. Chem.* **1996**, *47*, 18290. (b) Gu, Z. Z.; Sato, O.; Iyoda, T.; Hashimoto, K.; Fujishima, A. *Chem. Mater.* **1997**, *9*, 1092.

(11) Olabe, J. A.; Ayamonino, P. J. *J. Inorg. Nucl. Chem.* **1974**, *36*, 1221–1226.

Table 1. Crystal Data and Numerical Details of the Structure Determination of $(PPh_4)_2[Fe(CN)_5C_3H_4N_2]\cdot 2H_2O$ and $Na_3[Fe(CN)_5(en)]\cdot 5H_2O$

	$(PPh_4)_2[Fe(CN)_5(im)]\cdot 2H_2O$	$Na_3[Fe(CN)_5(en)]\cdot 5H_2O$
formula	$2(C_{24}H_{20}P)\cdot(C_8H_4N_7Fe)\cdot 2(H_2O)$	$3Na\cdot(C_7H_8N_7Fe)\cdot 5(H_2O)$
fw (g mol^{-1})	968.84	405.08
cryst syst	triclinic	monoclinic
space group	$P\bar{1}$	$P2_1/n$
a, b, c/Å	9.8108(15), 11.1655(17), 23.848(4)	8.3607(7), 11.1624(9), 17.4233(14)
α, β, γ/deg	87.219(2), 85.573(2), 70.729(2)	90.1293(9)
vol (Å^3)	2457.9(7)	1626.0(2)
Θ range unit cell: min−max (deg); reflns	2.49−28.94; 5165	2.70−29.46; 7779
Z	2	4
D_{calc} (g cm^{-3})	1.309	1.655
F(000)	1010	832
μ(Mo Kα) (cm^{-1})	4.22	10.4
color, habit	red-brown, parallelepiped	yellow, block
approx. cryst dimension, mm	0.53 × 0.38 × 0.32	0.49 × 0.34 × 0.23
temp (K)	100(1)	100(1)
R_F where $F_0 \geq 4\sigma(F_0)^a$	0.0514	0.0287
wR_2	0.1379	0.0745

^{a} $R_F = \sum(||F_o| - |F_c||)/\sum|F_o|$ and $wR_2 = [\sum[w(F_o^2 - F_c^2)^2]/\sum[w(F_o^2)^2]]^{1/2}$.

$C_8H_4ZnFeN_7.0.54(H_2O)$ (**3**): C, 28.48; H, 1.79; N, 29.06. Found: C, 28.81; H, 1.54; N, 29.05.

Mn(bpy)[Fe(CN)$_5$imidazole]·H$_2$O (4). A total of 3 mL of an aqueous solution containing $MnCl_2\cdot 4H_2O$ (30 mg) and 2,2′-bipyridine (24 mg) was layered gently at the bottom of a test tube. A total of 2 mL of water was added as a second layer, and a third layer of 4 mL of an ethanolic solution of $(Ph_4P)_2[Fe(CN)_5$-imidazole$]\cdot 2H_2O$ was carefully layered over the second layer. The solution was allowed to stand, and red brown platelet crystals of **4** were collected after 2 weeks (yield 90 mg). Anal. Calcd for $C_{18}H_{12}MnFeN_9.H_2O$ (**4**): C, 44.75; H, 2.92; N, 26.09. Found: C, 44.10; H, 2.53; N, 25.87.

Physical Measurements. IR spectra were recorded on a Perkin-Elmer spectrum 400 FT-IR machine equipped with a UATR accessory and MCT liquid-N$_2$-cooled detector in the range between 4000 and 600 cm^{-1}. Raman spectra were recorded using a Perkin-Elmer Raman station 400 on samples suspended in paraffin oil to minimize sample heating. UV/vis−NIR absorption spectra were recorded on a JASCO V-570 UV/vis−NIR spectrophotometer equipped with an integrating sphere for diffuse reflectance measurements. Samples were diluted in BaSO$_4$. Magnetic susceptibility measurements under an applied field of 100 G were carried out using a Quantum Design SQUID magnetometer in the temperature range 2−300 K. Magnetization versus magnetic field measurements in the field range of −10 000 to +10 000 Oe (∼−10 000 to +10 000 G) were carried out for **1** and **2** at 2 and 5 K, respectively. Diamagnetic corrections of the constituent atoms were applied to the empirical magnetic data of all samples. In all cases, batches of small crystals were employed to remove effects of crystal orientation.

X-Ray Crystallographic Data. All refinement calculations and graphics were performed on an HP XW6200 (Intel XEON 3.2 Ghz)/Debian-Linux computer with the program package SHELXL (least-squares refinements).[12] Crystals were mounted on glass fibers and cooled to 100(1) K using a Bruker KRYO-FLEX low-temperature device. Intensity measurements were performed using a graphite monochromated Mo Kα radiation source (λ = 0.71073 Å) from a sealed ceramic diffraction tube (SIEMENS). Crystal fragments of $(PPh_4)_2[Fe(CN)_5(im)]\cdot 2H_2O$ and $Na_3[Fe(CN)_5(en)]\cdot 5H_2O$, cut to size to fit in the homogeneous part of the X-ray beam, with dimensions of 0.53 × 0.38 × 0.32 mm and 0.49 × 0.34 × 0.23 mm, respectively, were mounted on top of a glass fiber and aligned on a Bruker[13] SMART APEX CCD diffractometer. The unit cell[14] was identified as triclinic, space group $P\bar{1}$ for $(PPh_4)_2[Fe(CN)_5(im)]\cdot 2H_2O$. The E-statistics were indicative of a centrosymmetric space group.[15] Reduced cell calculations did not indicate higher metric lattice symmetry.[16] Examination of the final atomic coordinates of the structure did not yield extra crystallographic or metric symmetry elements.[17,18] The hydrogen atoms of the phenyl groups for $(PPh_4)_2[Fe(CN)_5(im)]\cdot 2H_2O$ were generated by geometrical considerations, constrained to idealized geometries, and allowed to ride on the carrier atoms with an isotropic displacement parameter related to the equivalent displacement parameter of their carrier atoms. The unit cell[14] was identified as monoclinic for $Na_3[Fe(CN)_5(en)]\cdot 5H_2O$. The space group $P2_1/n$ was derived from the systematic extinctions. A difference Fourier synthesis resulted in the location of all of the hydrogen atoms, and isotropic displacement parameters were refined for $Na_3[Fe(CN)_5(en)]\cdot 5H_2O$. Crystallographic data and numerical details on the structure determination of $(PPh_4)_2[Fe(CN)_5(im)]\cdot 2H_2O$ and $Na_3[Fe(CN)_5(en)]\cdot 5H_2O$ are given in Table 1. Selected interatomic distances (Å) and bond angles (deg) for $(PPh_4)_2[Fe(CN)_5(im)]\cdot 2H_2O$ and $Na_3[Fe(CN)_5(en)]\cdot 5H_2O$ are represented in Tables 2 and 3, respectively. Tables of atom positions, displacement parameters, distances, and angles and tables of F_o^2, F_c^2 and $\sigma(F_o^2)$ are available in the Supporting Information.

The overall data collection time was 7.8 h for **1**, **3**, and **4** and 17.9 h for compound **2**. The crystal used in the experiment for compound **2** diffracted weakly; hence, a 30.0 s exposure time for each image was employed. The structures were solved by Patterson methods,[19] and extension of the model was accomplished by direct methods applied to difference structure factors using the program DIRDIF-08. Final refinement on F^2 was carried out by full-matrix least-squares techniques. The positional and (an)isotropic displacement parameters for the non-hydrogen atoms were refined on F^2 with full-matrix least-squares procedures minimizing the function $Q = \sum_h[w(|(F_o^2) - k(F_c^2)|)^2]$, where $w = 1/[\sigma^2(F_o^2) + (aP)^2 + bP]$, $P = [\max(F_o^2,0) + 2F_c^2]/3$, and F_o and F_c are the observed and calculated structure factor amplitudes, respectively. Apart from the hydrogen of solvate water molecules in **3**, which were not detected, the hydrogen atoms were generated

---

(12) Sheldrick, G. M. *Acta Crystallogr.* **2009**, *A64*, 112x.

(13) *SMART, S, SADABS Area Detector Control and Integration Software. Smart Apex Software Reference Manuals*; Bruker Analytic X-ray Instruments, Inc.: Madison, WI, 2007.

(14) Duisenberg, A. J. M. *J. Appl. Crystallogr.* **1992**, 92–96.

(15) Snow, M. R.; Tiekink, E. R. T. *Acta Crystallogr., Sect. B* **1988**, 676–677.

(16) Spek, A. L. *J. Appl. Crystallogr.* **1988**, 578–579.

(17) Le Page, Y. *J. Appl. Crystallogr.* **1987**, 264–269.

(18) Le Page, Y. *J. Appl. Crystallogr.* **1988**, 983–984.

(19) Beurskens, P. T.; Beurskens, G.; de Gelder, R.; Smits, J. M. M.; Garcia-Granda, S.; Gould, R. O. *The DIRDIF-08 program*; Crystallography Laboratory, University of Nijmegen: The Netherlands, 2008.

Table 2. Selected Interatomic Distances (Å) and Bond Angles (deg) of $(PPh_4)_2[Fe(CN)_5(im)]\cdot 2H_2O$

Fe−N6	1.999(2)	N6−C6	1.335(4)
Fe−C1	1.964(3)	N6−C8	1.382(4)
Fe−C2	1.934(3)	N7−C6	1.339(4)
Fe−C3	1.936(3)	N7−C7	1.365(4)
Fe−C4	1.961(3)	C7−C8	1.360(4)
Fe−C5	1.936(3)	N1−C1	1.160(3)
C1−Fe−C2	91.01(11)	C1−Fe−C3	86.75(12)
C1−Fe−C4	176.53(13)	C1−Fe−C5	93.01(11)
N6−Fe−C1	89.54(11)	N6−Fe−C3	176.11(10)
N6−Fe−C5	91.03(11)	N6−Fe−C8	109.3(3)
N6−Fe−C4	92.89(11)	C2−Fe−C3	90.22(13)
C2−Fe−C5	175.50(12)	C2−Fe−C4	86.47(12)
C3−Fe−C4	90.87(12)	C3−Fe−C5	87.99(13)
Fe−N6−C8	127.09(19)	C4−Fe−C5	89.43(12)
Fe−N6−C6	127.17(19)	C6−N6−C8	105.4(2)
C6−N7−C7	107.9(3)	N6−C6−N7	111.0(3)
N7−C7−C8	106.4(3)	N6−C8−C7	109.3(3)
Fe−C1−N1	178.7(3)		

Table 3. Selected Interatomic Distances (Å) and Bond Angles (deg) of $Na_3[Fe(CN)_5(en)]\cdot 5H_2O$

Fe−N6	2.0843(13)	Fe−C5	1.9224(14)
Fe−C1	1.9379(14)	N6−C6	1.476(2)
Fe−C2	1.9330(14)	C6−C7	1.525(2)
Fe−C3	1.8658(14)	C7−N7	1.472(2)
Fe−C4	1.9159(14)	N1−C1	1.1661(19)
C1−Fe−C2	90.57(6)	C1−Fe−C4	176.71(6)
C1−Fe−C3	89.78(6)	C1−Fe−C5	89.09(6)
N6−Fe−C1	93.68(5)	N6−Fe−C3	176.48(6)
N6−Fe−C2	89.94(5)	N6−Fe−C4	87.16(6)
N6−Fe−C3	176.48(6)	N6−Fe−C5	89.83(5)
C2−Fe−C3	89.36(6)	C2−Fe−C4	92.62(6)
C2−Fe−C5	179.57(6)	C3−Fe−C4	89.43(6)
C3−Fe−C5	90.89(6)	C4−Fe−C5	87.73(6)
Fe−N6−C6	119.72(10)	N6−C6−C7	113.87(13)
N7−C7−C6	110.46(13)		

by geometrical considerations with an isotropic displacement parameter. Crystal data and numerical details on data collection and refinement for **1**, **2**, **3**, and **4** are summarized in Table 4. Selected bond distances and angles are provided as Supporting Information.

CIF files for all structures can be obtained free of charge via www.ccdc.cam.ac.uk/ or from the Cambridge Crystallographic Data Centre, 12 Union Road, Cambridge CB2 1EZ, United Kingdom (fax: (+44) 1223-336-033 or e-mail: deposit@ccdc.cam.ac.uk). CCDC numbers $(PPh_4)_2[Fe(CN)_5(im)]\cdot 2H_2O$ (both 783155 and 783156), $Na_3[Fe(CN)_5(en)]\cdot 5H_2O$ (783154), **1** (783157), **2** (783161), **3** (783159), and **4** (783160 at 100 K, also 783158 at 224 K) contain crystallographic data. These data can be obtained free of charge via www.ccdc.cam.ac.uk/ or from the Cambridge Crystallographic Data Centre, 12 Union Road, Cambridge CB2 1EZ, United Kingdom (fax: (+44) 1223-336-033 or e-mail: deposit@ccdc.cam.ac.uk).

Results and Discussion

Structural Characterization of $(PPh_4)_2[Fe(CN)_5(im)]\cdot 2H_2O$. $(PPh_4)_2[Fe(CN)_5(im)]\cdot 2H_2O$ was isolated by slow evaporation of a solution of $Na_3[Fe(CN)_5(en)]\cdot 5H_2O$ and tetraphenylphosphonium chloride in water as large red brown crystals.[20] These crystals have a triclinic unit cell with two molecules per unit cell. The asymmetric unit contains one formula unit, consisting of five moieties: an anionic Fe complex, two tetraphenylphosphonium cations, and two water molecules. These moieties are linked by hydrogen bonds, forming an infinite two-dimensional network along the base vectors [1 0 0] and [0 1 0]. The solid state structure of complex $(PPh_4)_2[Fe(CN)_5(im)]\cdot 2H_2O$ is shown in Figure 2. It consists of five cyano (CN^-) ligands and one imidazole ($C_3H_4N_2$) ligand coordinated to the iron center (Fe^{III}). Four of the CN^- ligands are in the equatorial plane, while the fifth CN^- ligand is collinearly axial with the imidazole group. Two $[Fe(CN)_5(im)]^{2-}$ moieties are bonded together through a H bond in N7−H7···N3, forming asymmetric chains along the *c* axis and separated by two PPh_4 cations.

The Fe−C bond lengths are between 1.934(3) and 1.964(3) Å, as expected for a low-spin Fe^{III} mononuclear complex (e.g., $[Fe^{III}(CN)_6]^{3-}$ (1.927(14)−1.971(19) Å)[21]), and are also in good agreement with those reported for $Rb_2[Fe^{III}(CN)_5NO]$ (1.92(2) Å−1.96(2) Å).[22] The structure shows that the tetraphenylphosphonium cations are not involved to an appreciable extent in bonding with either H_2O or the $[Fe(CN)_5(im)]^{2-}$ ions. Ph_4P^+ cations have been reported to stabilize the crystal lattice of low-spin Fe^{III} complexes of the type $PPh_4[Fe(CN)_4bipy]\cdot 2H_2O$ (bipy = 2,2′-bipyridine) and $PPh_4[Fe(CN)_4phen]\cdot 2H_2O$ (phen = 1,10-phenanthroline).[23,24]

Structural Characterization of $Na_3[Fe(CN)_5(en)]\cdot 5H_2O$. Compound $Na_3[Fe(CN)_5(en)]\cdot 5H_2O$ was obtained by ligand substitution (NO) of $[Fe(CN)_5NO]^{2-}$ using an excess of ethylenediamine. Yellow crystals suitable for X-ray diffraction were obtained upon standing and were comprised of a monoclinic unit cell containing four formula units. The asymmetric unit consists of mononuclear $[Fe(CN)_5(en)]^{3-}$ cations, three sodium cations, and five water molecules. These moieties are linked by hydrogen bonding, forming an infinite three-dimensional network along the base vectors [1 0 −1], [0 0 2], and [0 1 1]. The structure of $[Fe(CN)_5(en)]^{3-}$ is shown in Figure 3.

As expected, $Na_3[Fe(CN)_5(en)]\cdot 5H_2O$ consists of five cyano (CN^-) ligands and one ethylendiamine ($C_2H_8N_2$) ligand coordinated to an iron(II) center. Four of the cyano groups are situated in the equatorial plane, while one cyano is axially collinear with the ethylenediamine group. The Fe−N bond length (of the ethylene diamine group) in $Na_3[Fe(CN)_5(en)]\cdot 5H_2O$ is 2.0843(13) Å, which is comparable to that reported[25] for $Na_3[Fe^{II}(CN)_5NH_3]\cdot 7H_2O$ (2.071(2) Å). The length of the Fe−C bond *trans* to the ethylene diamine ligand is 1.8658(14) Å, which is 0.07 Å shorter than the Fe−C bonds in the equatorial positions. This difference was found to be 0.06 Å for $Na_3[Fe^{II}(CN)_5NH_3]\cdot 7H_2O$ and 0.05 Å for $[Et_4N]_3[Fe^{II}(CN)_5py]$.[26] This difference reflects the relative donor strength of the ethylene diamine and cyanides as ligands. Ethylene diamine promotes the π-back-bonding from an electron-rich metal to the π-acceptor cyanide in the *trans* position. Indeed, the difference can be compared with that reported for $Na_2[Fe(CN)_5MeQ^+]$

---

(20) A study of the mechanism for the formation of the imidazole ring from ethylene diamine will be reported elsewhere.

(21) Vannerberg, N. G. *Acta Chem. Scand.* **1972**, *26*, 2863–2876.

(22) Soria, D. B.; Amalvy, J. I.; Piro, O. E.; Castellano, E. E.; Aymonino, P. J. *J. Chem. Crystallogr.* **1996**, *26*, 325–330.

(23) Lescouëzec, R.; Lloret, F.; Julve, M.; Vaissermann, J.; Verdaguer, M.; Llusar, R.; Uriel, S. *Inorg. Chem.* **2001**, *40*, 2065–2072.

(24) Lescouëzec, R.; Lloret, F.; Julve, M.; Vaissermann, J.; Verdaguer, M. *Inorg. Chem.* **2002**, *41*, 818–826.

(25) Parise, A. R.; Piro, O. E.; Castellano, E. E.; Olabe, J. A. *Inorg. Chim. Acta* **2001**, *319*, 199–202.

(26) Chiarella, G. M.; Melgarejo, D. Y.; Koch, S. A. *J. Am. Chem. Soc.* **2006**, *128*, 1416–1417.

Table 4. Crystallographic Data for $Co(H_2O)_2[Fe(CN)_5imidazole]\cdot 2H_2O$ (**1**), $Mn(CH_3OH)_2[Fe(CN)_5imidazole]$ (**2**), $Zn[Fe(CN)_5imidazole]\cdot H_2O$ (**3**), and $Mn(bpy)[Fe(CN)_5imidazole]\cdot H_2O$ (**4**)

	1	2	3	4
formula	$C_8H_8CoFeN_7O_2.2(H_2O)$	$C_{10}H_{12}FeMnN_7O_2$	$C_8H_4FeN_7Zn.0.54(H_2O)$	$C_{18}H_{12}FeMnN_9.H_2O$
mw, g mol^{-1}	385.03	373.03	328.13	483.17
cryst syst	orthorhombic	orthorhombic	orthorhombic	orthorhombic
temp, K	100(1)	100(1)	100(1)	100(1)
space group	*Imma*, 74	$P2_12_12_1$, 19	*Pnma*, 62	*Pnma*, 62
a, Å	7.3558(10)	7.385(5)	13.783(2)	13.192(3)
b, Å	14.627(2)	13.767(9)	7.1672(11)	7.2242(16)
c, Å	14.909(2)	14.895(10)	12.599(2)	22.294(5)
V, Å^3	1604.1(4)	1514.4(18)	1244.6(3)	2124.7(8)
ρ_{calc}, g cm^{-3}	1.594	1.636	1.747	1.511
Z	4	4	4	4
Θ range unit cell: min−max, deg	2.73−29.04	2.73−21.81	2.96−27.44	2.96−25.18
reflns	2099	444	3238	2654
λ, Å	0.71073	0.71073	0.71073	0.71073
spaceGroup_*Z*	16	4	8	8
F(000), electrons	776	752	644	976
μ, cm^{-1}	19.62	18.05	30.85	13.06
color, habit	red, block	red, block	red, octahedron	red, platelet
approx cryst dimensions, mm	0.29 × 0.25 × 0.15	0.17 × 0.15 × 0.12	0.39 × 0.23 × 0.15	0.23 × 0.11 × 0.04
Θ: min, max/deg	2.73, 27.09	2.73, 21.72	2.96, 26.36	2.96, 25.02
index ranges	$-9 \le h \le 9; -18 \le k \le 18; -17 \le l \le 19$	$-7 \le h \le 7; -14 \le k \le 14; -15 \le l \le 15$	$-15 \le h \le 17; -8 \le k \le 8; -15 \le l \le 15$	$-15 \le h \le 15; -8 \le k \le 8; -26 \le l \le 26$
GoF	1.135	1.122	1.063	1.071
$R(F)$	0.0433	0.0705	0.0279	0.0429
$wR(F^2)$	0.1186	0.1768	0.0751	0.1159
largest diff, peak and hole, e/Å^3	−0.38, 2.14(14)	−0.6, 1.7(3)	−0.32, 0.83(9)	−0.41, 0.67(9)

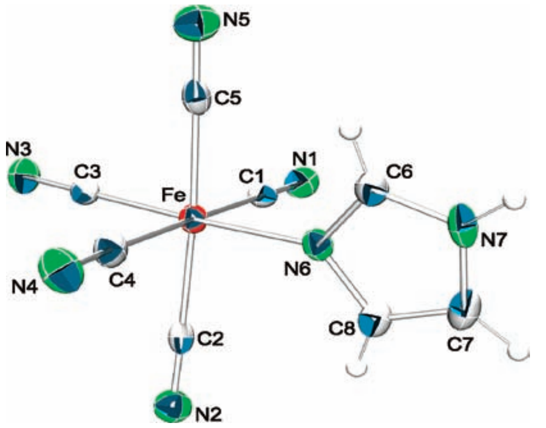

Figure 2. Structure of the anion in $(PPh_4)_2[Fe(CN)_5(im)]\cdot 2H_2O$. Counterions and solvent are omitted for clarity.

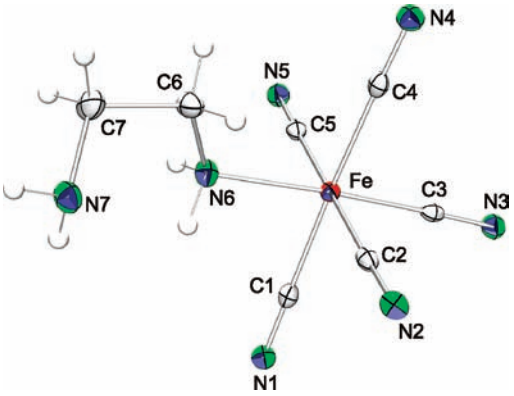

Figure 3. Structure of $Na_3[Fe(CN)_5(en)]\cdot 5H_2O$. Counterions and solvent of crystallization are omitted for clarity.

(0.03 Å; where MeQ^+ is *N*-methyl-4,4′-bipyridinium),[27] which is less, possibly due to the stronger π-acceptor capability of the MeQ^+ ligand compared to ethylene diamine or ammonia.

Description of the Structures 1−4. Single crystals of materials **1**−**4** were obtained in general by the slow diffusion of solvents. For each complex, several approaches to crystallization were attempted until crystals suitable for X-ray diffraction analysis were obtained.

Structure of $Co(H_2O)_2[Fe(CN)_5imidazole]\cdot 2H_2O$ (1). $Co(H_2O)_2[Fe(CN)_5imidazole]\cdot 2H_2O$ (**1**) crystallizes in the orthorhombic space group *Imma* with four formula units in the unit cell (Figure 4). The structure of **1** is made up of neutral dinuclear entities of the formula $[Co^{II}(H_2O)_2(Fe^{III}(CN)_5im)]$. The unit $[Fe^{III}(CN)_5imidazole]^{2-}$ acts as a monodentate ligand to four *trans*-diaquacobalt(II) units through its four cyanide groups in equatorial positions; the *axial* cyanide ligand does not act as a bridging ligand. This leads to a two-dimensional system with basic square $[Co_2Fe_2(CN)_4]$ structural motifs running parallel the *a* and *b* axes. This is different from that reported for $Co[Fe(CN)_5NO]$,[28] which crystallizes in a face-centered space group forming a three-dimensional network with all five cyanide ligands acting as bridges between iron and cobalt ions, and with the cobalt coordinated to one water molecule.

The average of N−Co and O−Co distances in **1** are 2.107(2) and 2.119(9) Å, respectively, forming a bipyramidal shape with the N−Co bond constituting the planar base. The Fe ion is coordinated to cyanide ligands and one N atom from the imidazole ligand. The Fe−N bond (1.958(5) Å) with the imidazole is affected by π-back-bonding, which

---

(27) Coe, B. J.; Harries, J. L.; Helliwell, M.; Jones, L. A.; Asselberghs, I.; Clays, K.; Brunschwig, B. S.; Harris, J. A.; Garin, J.; Orduna, J. *J. Am. Chem. Soc.* **2006**, *128*, 12192–12204.

(28) Mullica, D. F.; Tippin, D. B.; Sappenfield, E. L. *J. Coord. Chem.* **1991**, *24*, 83.

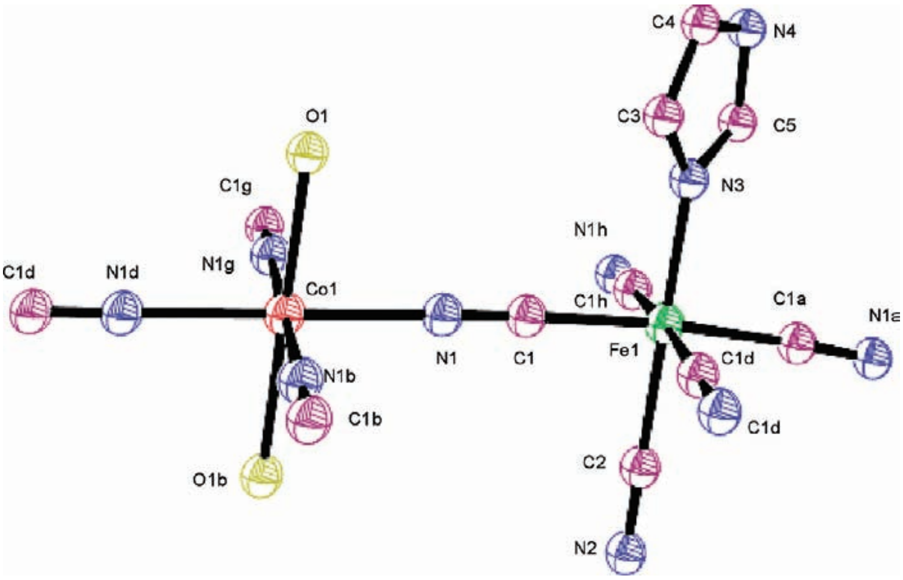

Figure 4. Structure of the **1**. Thermal ellipsoids are drawn at the 50% probability level.

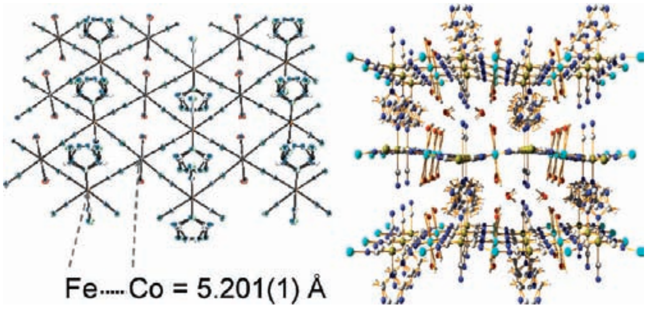

Figure 5. Extended crystal structure of **1** with a view (left) onto the 2-D layers and (right) stacking along the *a* axis.

results in shortening by 0.032 Å of the $Fe-C_{trans}$ bond (from the CN situated trans to the imidazole) compared to the other $Fe-C_{eq}$ bonds (1.951(3) Å). This leads to the distortion of the octahedral arrangement around the Fe ions, with the iron center located above the plane of the equatorial cyano ligands toward the imidazole ($N-Fe-C_{eq} > 90°$, $C_{eq}-Fe-C_{trans} < 90°$). The presence of two different types of octahedra around the Fe and Co cations results in a serpentine arrangement of the crystal lattice (Figure 5). The serpentine appearance of the structure is also due to the deviation in planarity, which is associated with the divergence of the Co−N−C angle from 180° (178.8(2)°) compared to that of the $N-C_{eq}-Fe$ angle (177.7(3)°).

The interlayer is occupied by overlapping imidazole ligands from each plane along the *a* axis and by water molecules. The interplanar imidazole−imidazole distance is 3.683 Å. The intramolecular Fe−Co distance through the cyano bridges is 5.201(1) Å, whereas the shortest interlayer metal−metal distances are 7.725(2) Å for Fe···Fe, 8.312(2) Å for Co···Co, and 7.957 Å and 8.312(2) Å for Fe···Co. Adjacent layers are connected through hydrogen bonds, yielding a quasi-3D network, i.e., hydrogen bonding between interlayer water molecules and the nonbridging *trans*-cyanide of the Fe ion of one layer and nitrogen of the imidazole ligand, as shown in Figure 6. The H-bond distances are 2.806(3) for $O_{Co}\cdots O_{H_2}O$, 3.032(9) Å for $O_{Co}\cdots N_{im}$, and 2.999(4) Å for $O_{H_2}O-N_{CNtrans}$.

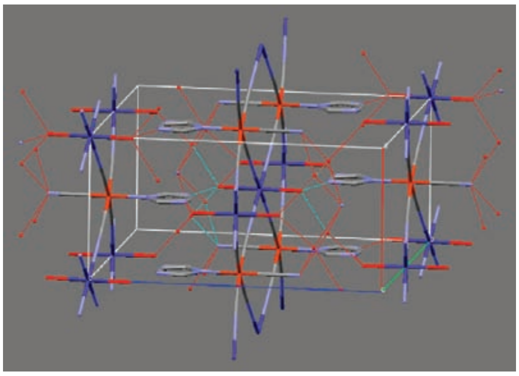

Figure 6. Fragment of the structure of **1** showing the network on hydrogen bonding (dotted lines) between coordinated water molecules (on the Co cation), water molecules of crystallization, and the *trans*-cyanide of Fe and N of imidazole.

Structure of $Mn(CH_3OH)_2[Fe(CN)_5imidazole]$ (2). The complex $Mn(CH_3OH)_2[Fe(CN)_5imidazole]$ crystallizes in the orthorhombic space group $P2_12_12_1$ with four formula units in the unit cell (Figure 7). An extended two-dimensional neutral network is formed by cyclic tetrameric $[-Mn-NC-Fe-]_2$ units with Fe and Mn atoms at the corners of a deformed square grid along the *ab* plan (Figure 8). This is in contrast to $Mn[Fe(CN)_5NO]\cdot xH_2O$, which, although it has been reported to crystallize in either the monoclinic[29] or orthorhombic[30] space group, shows a three-dimensional network structure with all five cyanides bridging the manganese and iron ions. In **2**, the $[Fe(CN)_5imidazole]^{2-}$ anions are connected to four $Mn(CH_3OH)_2^{2+}$ cations through the four equatorial CN^- ligands, while $Mn(CH_3OH)_2^{2+}$ cations are coordinated to four $[Fe(CN)_5imidazole]^{2-}$ anions through the nitrogen atom of the equatorial CN^- ligands.

The $[Fe(CN)_5imidazole]^{2-}$ ions exhibit a distorted octahedral configuration of ligands around the iron with the

---

[29] Mullica, D. F.; Tippin, D. B.; Sappenfield, E. L. *Inorg. Chim. Acta* **1990**, *174*, 129.

[30] Benavente, A.; A de Morán, J.; Piro, O. E.; Castellano, E. E.; Aymonino, P. J. *J. Chem. Crystallog*. **1997**, *27*, 343.

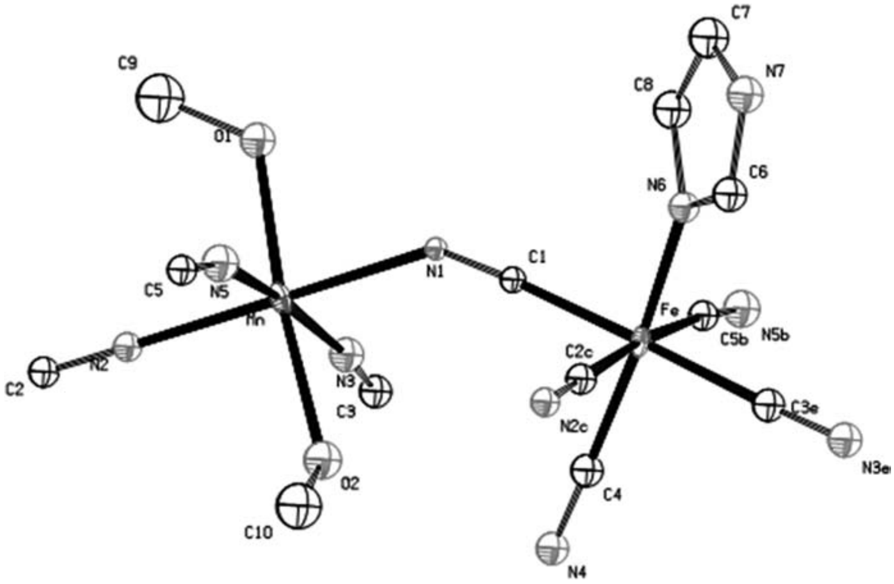

Figure 7. Structure of **2**. Thermal ellipsoids are drawn at 50% probability level.

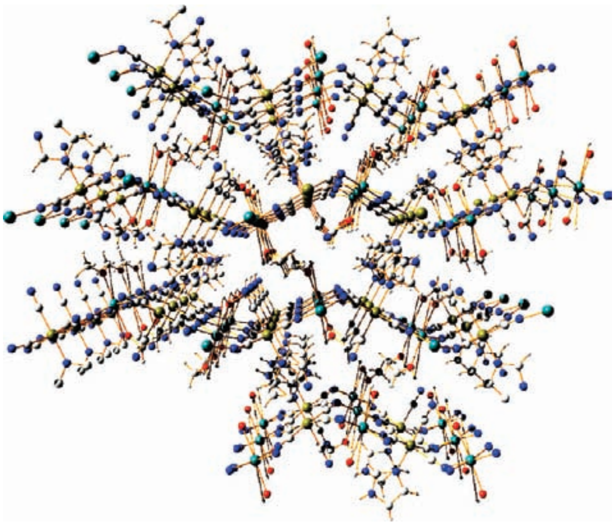

Figure 8. Perspective view of **2** along the *a* axis. The metal centers are represented in blue (Mn) and olive (Fe).

four symmetrically equivalent equatorial bridging CN^- ligands slightly bent toward the axial cyanide (opposite the imidazole group). The average Fe−C and Fe−N bond lengths are 1.937(17) and 1.958(8) Å, respectively.

The Mn^{II} ion is in an octahedral environment coordinated to four equatorial cyanides via the nitrogen and to two axial oxygen atoms from methanol with average Mn−N and Mn−O bond distances of 2.203(13) and 2.20(4) Å, respectively. Due to the nonplanarity (Figure 8) of the structure, the metal−metal (Mn···Fe) bond intralayer distances are irregular and vary between 5.006(4) and 5.288(15) Å and distances of 7.532(6) Å (Fe···Fe) and 8.818(7) Å (Mn···Mn) between two adjacent layers.

Structure of Zn[Fe(CN)$_5$imidazole]·H$_2$O (3). Zn[Fe(CN)$_5$imidazole]·H_2O crystallizes in the orthorhombic space group *Pnma* with four formula units in the unit cell (Figure 9). X-ray crystallographic analysis reveals that **3** is composed of a 3D coordination network (Figure 10). The view along the *b* axis shows formation of an irregular basic square with a $Zn_2Fe_2(CN)_4$ structural motif. The N−Zn−N (86.20(8)° and 88.56(8)°) and C−Fe−C (92°) angles form a distorted square. The $[Fe(CN)_5imidazole]^{2-}$ unit is a distorted octahedral complex with an Fe−N bond distance of 1.966(3) Å and a $Fe-C_{trans}$ bond equal to 1.919(4) Å, which is shorter than the other $Fe-C_{eq}$ bond distances (1.942(2) Å). The $[Fe(CN)_5imidazole]^{2-}$ moiety acts as a penta-monodentate ligand toward the zinc atoms through its five cyanide ligands. The zinc atom is pentacoordinated by five cyano nitrogens. The irregular value of Zn−N−C angles (155.7(3), 174.4(2), and 175.7(2)°) results in a distorted ZnN_5 square pyramidal structure around the Zn atom. The values of the metal−metal Fe···Zn bond distances are 4.97(1) Å through the axial CN, 5.135(1) Å, and 5.836(1) Å through the equatorial CN, which are comparable with that reported for $Zn^{II}[Fe^{III}(CN)_4$phenanthroline]·$4H_2O$ (5.132 and 5.187 Å).[31] Two nitrogens in

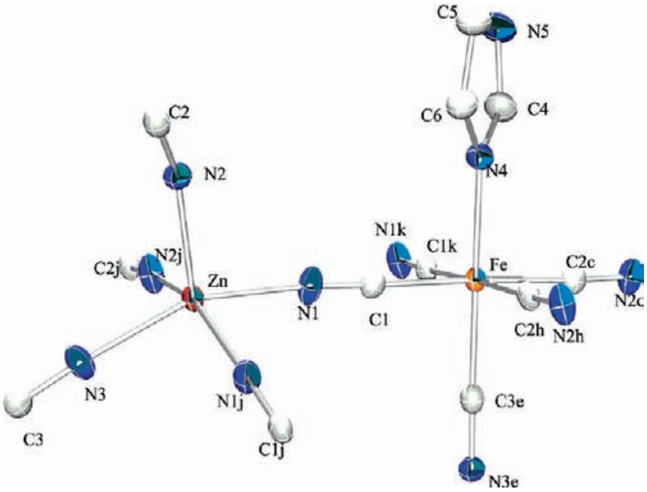

Figure 9. Structure of Zn[Fe(CN)$_5$imidazole]·H_2O (**3**). Thermal ellipsoids are drawn at the 50% probability level.

---

[31] Lescouëzec, R.; Lloret, F.; Julve, M.; Vaissermann, J.; Verdaguer, M.; Llusar, R.; Uriel, S. *Inorg. Chem.* **2001**, *40*, 2065.

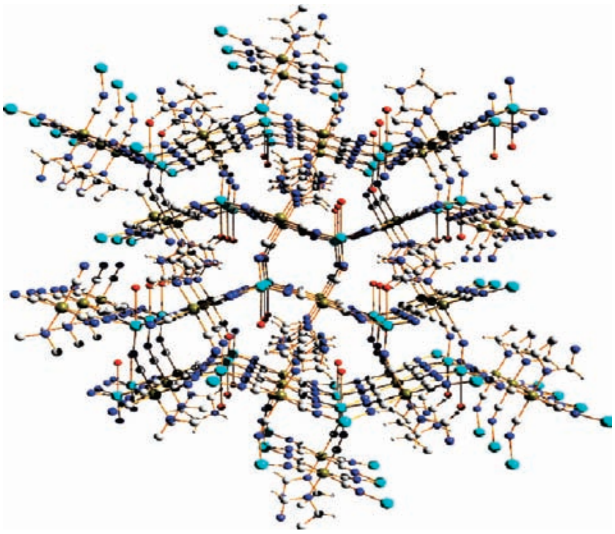

Figure 10. Perspective view of **3** along the *b* axis. The metals are represented in dark blue (Zn) and light blue (Fe).

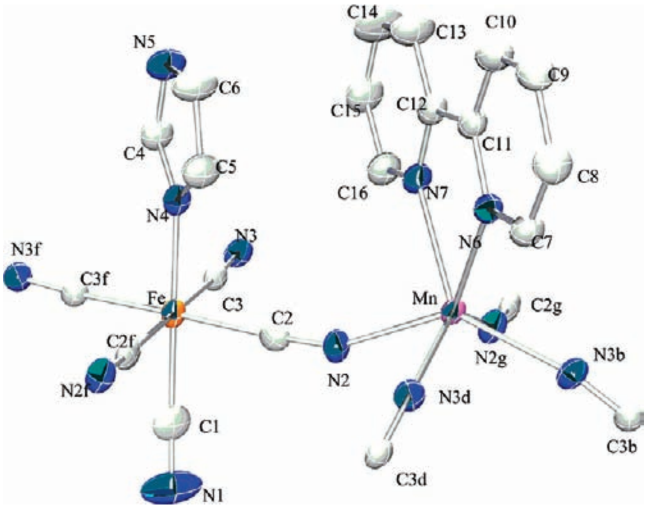

Figure 11. Structure of Mn(bpy)[Fe(CN)$_5$imidazole].H$_2$O (**4**). Thermal ellipsoids are drawn at the 50% probability level.

the longest edges of the tetranuclear unit form hydrogen bonds with water molecules.

Structure of Mn(bpy)[Fe(CN)$_5$imidazole]·H$_2$O (4). Mn(bpy)[Fe(CN)$_5$imidazole]·H$_2$O crystallizes in the orthorhombic space group *Pnma* with four formula units in the unit cell. The structure of **4** is comprised of one central [Fe(CN)$_5$imidazole]$^{2-}$ anion linked to four Mn(bpy)$^{2+}$ cations through its four equatorial CN$^-$ ligands, forming an extended two-dimensional network along the *a* and *b* axes (Figure 11). The network system is formed by cyclic [−Mn−CN−Fe−]$_2$ units of deformed square grids with metal atoms at the corners. The Fe site exhibits a distorted octahedral geometry. The average Fe−C$_{\text{trans}}$ bond distance is 1.9440(15) Å, whereas that of Fe−C$_{\text{ax}}$ is 1.927(6) Å, which is shorter due it being trans to the imidazole ligand. The Fe−N bond distance is 1.969(4) Å. The Mn ion is bonded to four equatorial CN$^-$'s via N and to the two N's of the bipyridine ligand with average bond lengths of 2.221(4) and 2.30(4) Å, respectively. The environment around the Mn ion is distorted octahedral, with the four N's of the CN resulting in a sinusoidal shape to the layers with Mn−N2−C2, 157.6(2)°, and Mn−N3−C3, 163.2(3)° (Figure 12). The Fe−Mn distance is 5.1930(14) Å.

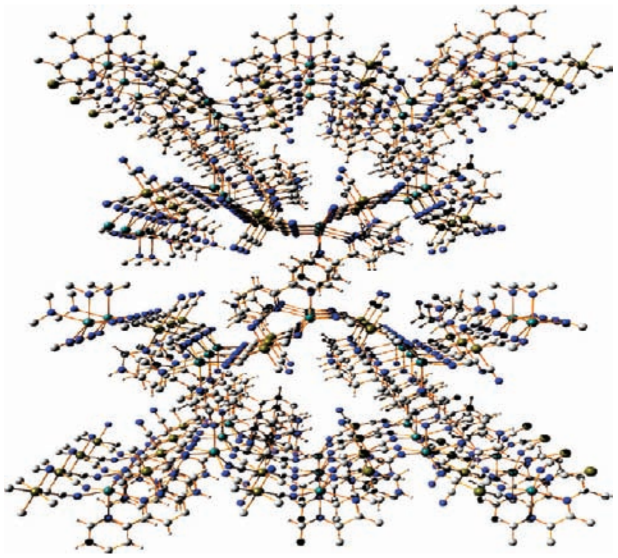

Figure 12. Perspective view of **4** along the *b* axis. The metals are represented in blue (Mn) and olive (Fe).

The deformed planes are antiparallel to each other, and the neighboring sheets overlap along the *b* axis via the bipyridine ligands, which are separated by 3.66 Å. The intrachain metal−metal separations through the bridging CN ligand are 5.193−5.298 Å. The shortest interlayer separation of the two adjacent metal cations (Mn···Mn) is 8.738(2) Å, whereas the longest separation is 11.719 Å (Fe···Fe).

FTIR and Raman Spectroscopy. The FTIR and Raman spectra of complexes recorded in the 4000−500 cm^{-1} range are shown in Figure 13. Their spectra show the bands of the imidazole ligand at 3364 cm^{-1} (υN−H), 3145 cm^{-1} (υC−H), 1539 cm^{-1}, 1507 cm^{-1}, 1428 cm^{-1}, 1323 cm^{-1}, 1178 cm^{-1} and 1064 cm^{-1} (υ_{ring}), 1260 cm^{-1} (δN−H), 1120 cm^{-1}, 1098 cm^{-1} (δC−H), and 756 cm^{-1} (γC−H), comparable to the data reported for imidazole complexes of the type [M(Him)$_6$](NO$_3$) and [M(Him)$_6$](ClO$_4$)$_2$ (M = Co, Ni, Fe, and Zn).[32] The bridging by the CN$^-$ ligands in the mixed metal systems presented here is confirmed by variation observed in the CN$^-$ stretching frequencies in the range of 2200−2000 cm^{-1} (Table 5).[33] In the FTIR spectra of the complexes, absorptions are observed at 2153 and 2115 cm^{-1} (**1**), 2145 and 2075 cm^{-1} (**2**), 2167 cm^{-1} (**3**), and 2146 and 2116 cm^{-1} (**4**). Overall, the absorptions are at higher wavenumbers than the cyano stretching vibrations of (Ph$_4$P)$_2$[Fe(CN)$_5$imidazole]·2H$_2$O (2104 and 2122 cm^{-1}). The higher frequencies of υ_{CN} that appear at 2153, 2145, 2167, and 2146 cm^{-1} for complexes **1**, **2**, **3**, and **4**, respectively, are assigned to the stretching vibration of the equatorial CN$^-$ ligands that form the M−CN−M′ bridges. Since the CN$^-$ stretching frequencies of these CN groups depend on the electronegativity, crystal field stability, oxidation number,

---

(32) Hodgson, J. B.; Percy, G. C.; Thornton, D. A. *J .Mol. Struct.* **1980**, *66*, 81.

(33) Nakamoto, K. *Infrared and Raman of Inorganic and coordination compounds. Part B: Applications in coordination, organometallic and biorganic chemistry*, 5th ed.; Wiley: New York, 1997.

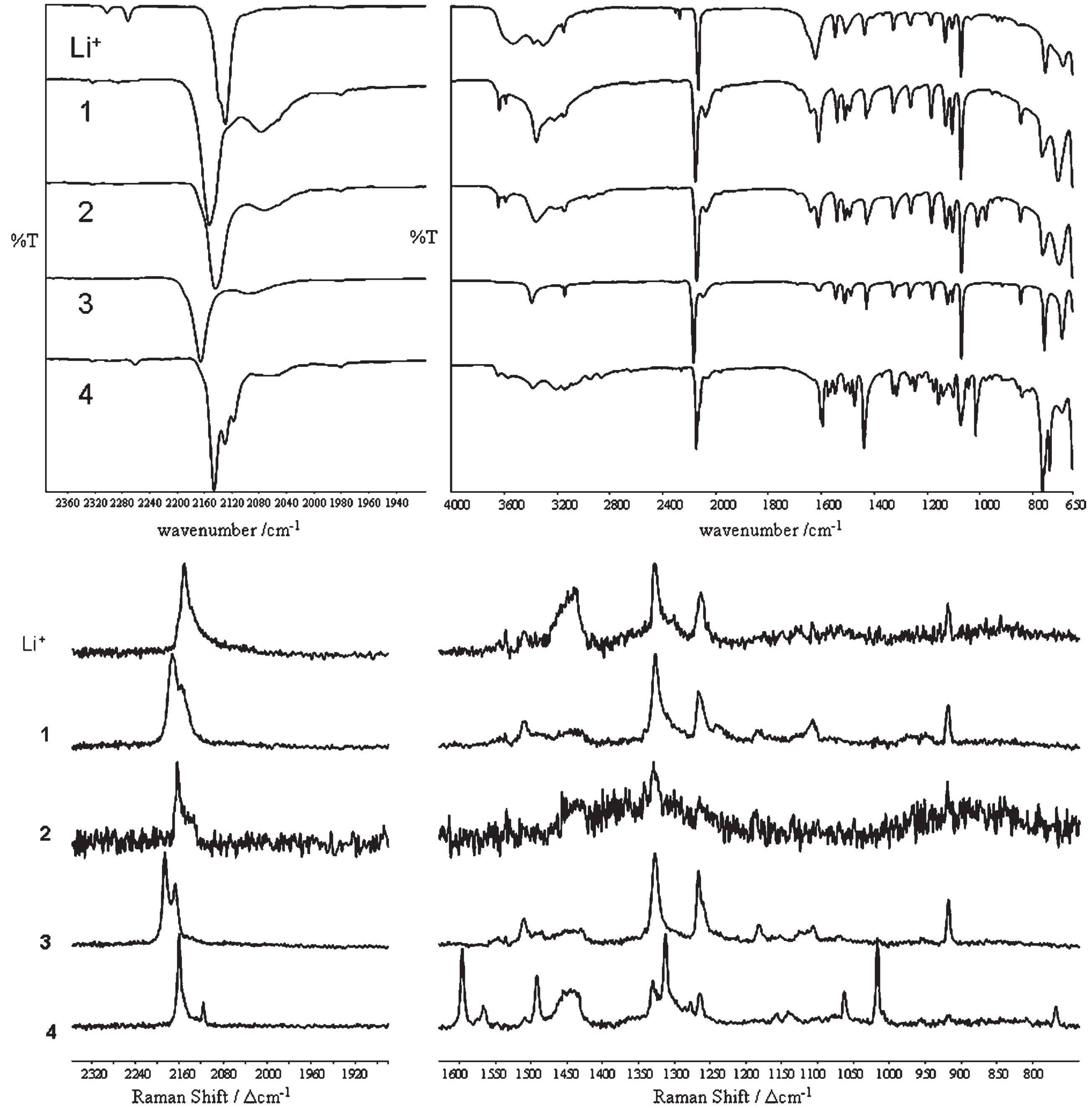

Figure 13. ATR-FTIR (upper) and Raman (λ_{exc} 785 nm, lower) spectra of the CN stretching region (left) and full spectrum (right) for **1**−**4** and $Li_2[Fe(CN)_5(imidazole)]$ (Li^+).

and coordination number of the metal ion,[34,35] then υCN of $Fe^{III}-CN-Zn^{II}$ > υCN of $Fe^{III}-CN-Co^{II}$ > υCN of $Fe^{III}-CN-Mn^{II}$ > υCN of $Fe^{III}-CN$. The frequencies at 2115 cm^{-1} (**1**) and 2116 cm^{-1} (**4**) are assigned as the nonbridging CN stretching vibrations by comparison with the complex $(PPh_4)_2[Fe(CN)_5(imidazole)]$.

The trends observed in the FTIR absorption spectra are observed also in the powder Raman spectra of the materials. In all cases, the Raman CN bands are at higher wavenumbers than those of the parent complex $(Ph_4P)_2[Fe(CN)_5imidazole]\cdot 2H_2O$ and are much less well-defined (Table 5). This is expected since the bulky PPh_4^+ cations serve to isolate the $Fe(CN)_5$imidazole core. Furthermore, for all of the bimetallic materials,

Table 5. FTIR and Raman CN Stretching Bands

	FTIR	Raman
1 (CoFe)	2151, 2145(sh), 2076	2169, 2151(sh)
2 (MnFe)	2143, 2070	2163, 2141 (sh)
3 (ZnFe)	2165, 2094	2186, 2168
4 ($Mn(bpy)_2Fe$)	2145, 2128, 2116, 2053	2160, 2116
5 (LiFe)	2138(sh), 2129	2150
$[PPh_4)_2[Fe(CN)_5$imidazole]	2129, 2121, 2104	2128, 2122, 2116, 2108

---

[34] Nakamoto, K. *Infrared and Raman Spectra of Inorganic and Coordination Compounds*, 4th ed.; Wiley: New York, 1986.

[35] Watzky, M. A.; Endicott, J. F.; Song, X.; Lei, Y.; Macatangay, A. *Inorg. Chem.* **1996**, *35*, 3463.

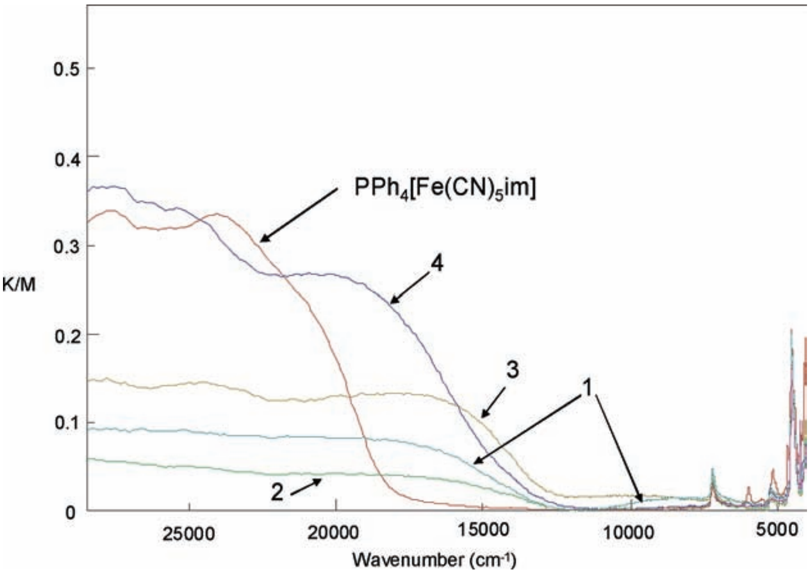

Figure 14. UV/Vis−NIR diffuse reflectance spectra of powdered samples diluted in $BaSO_4$.

the imidazole is oriented with its plane bisecting the x/y plane formed by the equatorial cyano ligands resulting in pseudo C_{4v} local symmetry. For the corresponding PPh_4^+ salt of $[Fe(CN)_5(imidazole)]^{2-}$, the imidazole is oriented such that the plane is coincident with the x/z molecular axis (and hence has C_{2v} local symmetry). For **4**, additional bands are observed corresponding to the 2-2′-bipyridine ligand coordinated to the manganese center.

UV/Vis−NIR Spectroscopy. The UV/vis−NIR diffuse reflectance spectra of all of the compounds as intimate mixtures in $BaSO_4$ are shown in Figure 14. $(Ph_4P)_2[Fe(CN)_5\text{-imidazole}]\cdot 2H_2O$ shows absorption bands in the solid state with maxima at 268, 356, and 415 nm and a shoulder at 528 nm. In the NIR region (1400−2500 nm), overtone IR absorption bands of cyano and PPh_4 moieties are observed. The absorption at ca. 400 nm is assigned as a LMCT band of the $[Fe(CN)_5\text{imidazole}]^{2-}$ by comparison with the solution spectrum of the complex. The spectra of the bimetallic complexes all show an absorption band at longer wavelengths compared to that of the $(Ph_4P)_2[Fe(CN)_5\text{imidazole}]\cdot 2H_2O$. In the visible region, a broad intense band is centered at ca. 645 nm for **1**, **2**, and **3** and at 580 nm for **4**. For **4**, an additional band at 302 nm (not shown) assigned to the $\pi-\pi^*$ transition of the bipyridine ligands is observed. The band at 645 nm is assigned as a LMCT transition of the $[Fe(CN)_5\text{imidazole}]^{2-}$, and the shift to longer wavelengths is attributed to stabilization of the Fe(III) d orbitals due to the weakening of the σ-donor properties of the CN^- ligands.

An additional weaker absorption in the near-red is observed for **1** and **3**. This band is absent in the spectra of the manganese complexes **2** and **4**. The observation of a near-IR absorption band for the Zn(II) complex as well as the Co(II) complex suggests that this band is not an intervalence charge transfer band. The red-shift in the main visible absorption band and the appearance of a weaker longer wavelength absorption is reminiscent of the absorption spectrum of $[Fe(CN)_5\text{imidazole}]^{2-}$ under basic conditions (i.e., a deprotonated imidazolato ligand) and reflects the stabilization of the Fe(III) d orbitals by reduction in the σ-donor strength of the cyano ligands that form the intermetal bridges.

Magnetic Properties of $(PPh_4)_2[Fe(CN)_5(im)]$, 1, 2, 3, and 4. The magnetic properties of **1**−**4** were investigated by temperature-dependent magnetic susceptibility measurements in the range of 2−300 K under an applied field of $H = 100$ Oe. In addition, field-dependent magnetization was determined at 2 K for **1** and 5 K for **2**. The magnitude of $\chi_M T$ of $(PPh_4)_2[Fe(CN)_5(im)]$ was determined between 5 and 300 K (Figure 15) and remains constant throughout. The effective magnetic moment was determined to be $\mu_{eff} = (8\chi_M T)^{1/2} = 1.71\ \mu_B$, which is typical for low-spin Fe^{III} ($S = 1/2$) complexes.

Figure 16 shows the temperature dependence of field-cooled and zero-field-cooled magnetization, $M(T)_{FC}$ and $M(T)_{ZFC}$, respectively, for **1** under an applied field of 100 Oe. The curves show a rapid increase at an ordering temperature of 25 K indicative of a magnetic transition. This ordering temperature is higher than that reported so far for $Co^{II}-Fe^{III}$ complexes of the type $A_xCo_y[Fe(CN)_6]_z\cdot nH_2O$ (between 0 and 16 K), where A is an alkali metal ion.[36] The temperature dependence of the magnetic susceptibility $\chi_M T(T)$ as well as $\chi^{-1}(T)$ plots are shown in Figure 17. The $\chi_M T$ value at 300 K is 3.22 $cm^3\ K\ mol^{-1}$ ($\mu_{eff} = 5.07\ \mu_B$) and is comparable to the theoretical value 3.00 $cm^3\ K\ mol^{-1}$ ($\mu_{eff} = 4.9\ \mu_{ss}$) for a ferromagnetic coupling between one Co^{II} high-spin and one Fe^{III} low-spin center. Upon cooling, $\chi_M T$ remains constant until 25 K, where it suddenly increases to reach a maximum value of 1445 $cm^3\ K\ mol^{-1}$ ($\mu_{eff} = 107.51\ \mu_B$) at 18 K and then decreases to 97.08 $cm^3\ K\ mol^{-1}$ ($\mu_{eff} = 27.86\ \mu_B$) at 2 K. This is in accord with the Currie−Weiss Law plot (based on $1/\chi_M = C(T - \theta)$) in the temperature range of 45−300 K, where a straight line with a positive Weiss

---

[36] (a) Sato, O.; Iyoda, T.; Fujishima, A.; Hashimoto, K. *Science* **1996**, *272*, 704. (b) Verdaguer, M. *Science* **1996**, *272*, 698. (c) Sato, O.; Einaga, Y.; Iyoda, T.; Fujishima, A.; Hashimoto, K. *J. Electrochem. Soc.* **1997**, *144*, L11. (d) Bleuzen, A.; Lomenech, C.; Escax, V.; Villain, F.; Varret, F.; Cartier dit Moulin, C.; Verdaguer, M. *J. Am. Chem. Soc.* **2000**, *122*, 6648. (e) Goujon, A.; Roubeau, O.; Varret, F.; Dolbecq, A.; Bleuzen, A.; Verdaguer, M. *Eur. Phys. J., B* **2000**, *14*, 115.

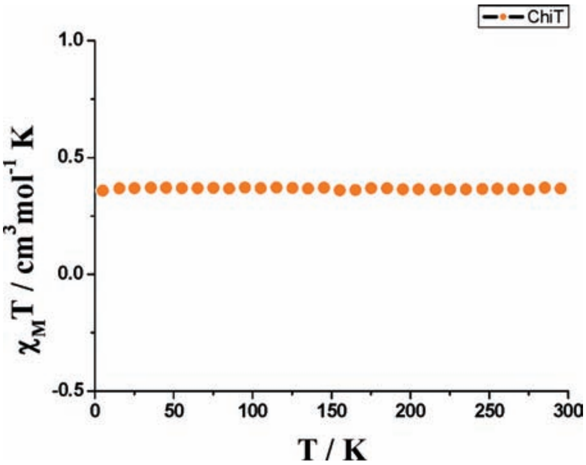

Figure 15. Temperature dependence of $\chi_M T$ of **1**.

constant of $\theta = +15.33$ K can be fit. The ferromagnetic behavior may be enhanced by the orthogonality of the half-filled orbitals of Fe^{III} ($(t_{2g})^1$) and Co^{II} ($(e_g)^2$).[37] The decrease of $\chi_M T$ below 18 K is assigned to an antiferromagnetic interlayer interaction since the interlayer distance (7.6−8.3 Å) is less than 10 Å.[38]

The field-dependent magnetization performed on **1** at 2 K (Figure 18) shows ferromagnetic behavior. Compound **1** reaches a saturation value of magnetization (3.21 Nμ_{ss}) close to the theoretical value of 4 Nμ_B for a bimetallic system of high-spin Co(II) and low-spin Fe(III). This is consistent with the parallel alignment of the interacting spins. The spectrum presents a hysteresis loop at 2 K with a coercive field (H_c) and a remnant magnetization (M_r) of 81 Oe and 2.81 Nμ_B, respectively. The high ordering temperature may be assigned to the dimensionality of the material, which facilitates cooperativity between metal centers along the planes compared to other reported Co/Fe bimetallics that crystallize as 3D systems in which defects in the structure serve to interrupt the cooperativity between metal centers. On the other hand, the position of the imidazole ligand in the structure is such that the superposition of different planes allows imidazoles from adjacent planes to orient parallel to each other to engage in $\pi-\pi$ stacking. The distance between the imidazoles rings is 3.683 Å, and hence $\pi-\pi$ interactions are not expected to be significant. However, an extensive network of hydrogen bonds between planes through water molecules and the presence of hydrogen bonds between the *trans*-CN, the imidazole ligand, and water of crystallization could influence the general magnetic properties of the complex.

The temperature dependence of the magnetization of **1** between 50 and 1000 Oe is shown in Figure 16. Similar behavior is observed at all field strengths with a sudden increase in the magnetization below 25 K up to a field-dependent maximum value between 3000 and 9600 emu mol^{-1} from 50 to 1000 Oe. The abrupt increase in the magnetization below 25 K confirms magnetic ordering arising from ferromagnetic coupling within each layer.

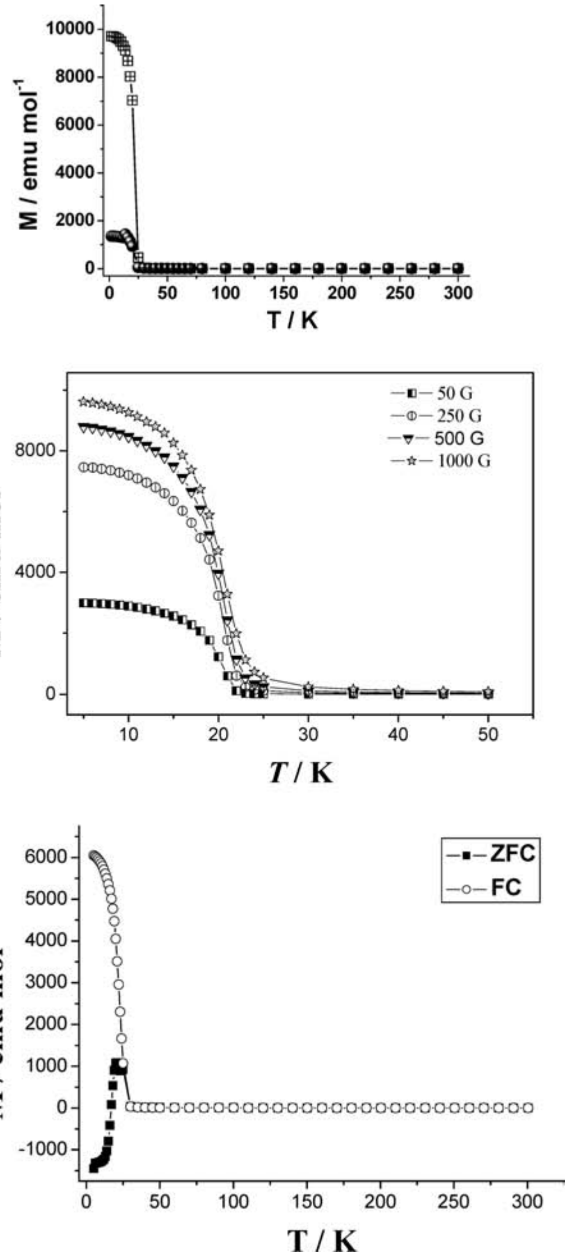

Figure 16. Temperature dependence of the magnetization of **1**. Upper graph: Field-cooled (FC, squares) and zero field-cooled (ZFC, circles) magnetization at 100 Oe. Middle graph: Under 50, 250, 500, and 1 kOe magnetic fields. Lower graph: Temperature dependence of the magnetization of dehydrated **1**. Field-cooled (FC, open circles) and zero-field-cooled (ZFC, black squares) magnetization at 100 Oe.

The role of water of crystallization in determining the magnetic properties of **1** was studied using dehydrated samples. The thermal dependence of the magnetic susceptibility $\chi_M T$ and $1/\chi$ for the dehydrated sample of **1** are shown in Figure 16. The ordering temperature is increased to 30 K from 25 K (for **1**). The positive Weiss constant for the dehydrated sample ($\theta = +12.26$ K, obtained between 50 and 300 K) is close to that of the hydrated sample (($\theta = +15.3$ K) and is indicative of ferromagnetic behavior. However, the zero-field-cooled (ZFC) and field-cooled (FC) magnetization measurements of dehydrated **1** (Figure 17) show a sharp rise below 30 K, indicative of a magnetic transition. The increase in the ordering temperature is tentatively assigned to a decrease in the interlayer separation due to the loss

---

[37] (a) Mallah, T.; Auberger, C.; Verdaguer, M.; Veillet, P. *J. Chem. Soc., Chem. Commun.* **1995**, 61. (b) Khan, O. In *Molecular Magnetism*; VCH: Weinheim, Germany, 1993.

[38] Ohba, M.; Fukita, N.; Ōkawa, H.; Hashimoto, Y. *J. Am. Chem. Soc.* **1997**, *119*, 1011.

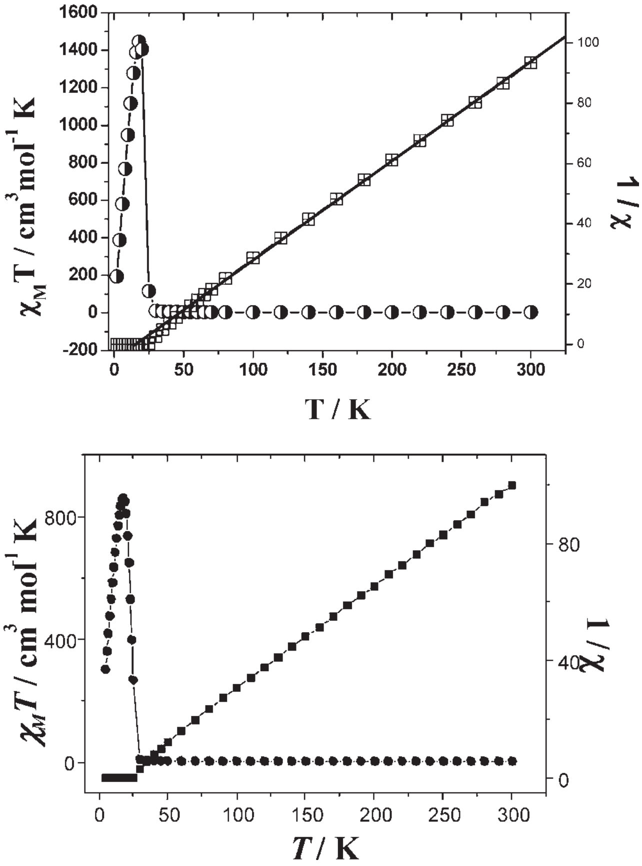

Figure 17. Temperature dependence of $\chi_M T$ (circles) and $1/\chi_M$ (squares) for (upper graph) **1** and dehydrated **1** (lower graph) at 100 Oe. The solid lines represent the Curie–Weiss law plot in the range of 50–300 K.

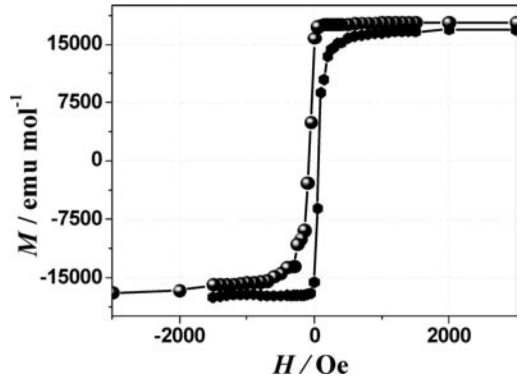

Figure 18. Field dependence of the magnetization of **1**.

of water of crystallization. A bifurcation of the curves is observed at 25 K, and the ZFC magnetization curve after reaching a maximum at 20 K rapidly decreases, which is indicative of domain wall freezing.[39]

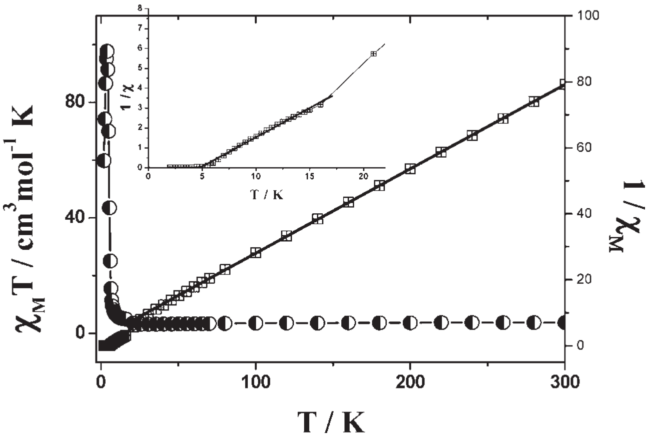

Figure 19. Temperature dependence of $\chi_M T$ (circles) and $1/\chi_M$ (squares) for **2** at 100 Oe. The solid line represents the Currie–Weiss law plot. Inset is the $1/\chi_M$ vs T plot between 0 and 22 K.

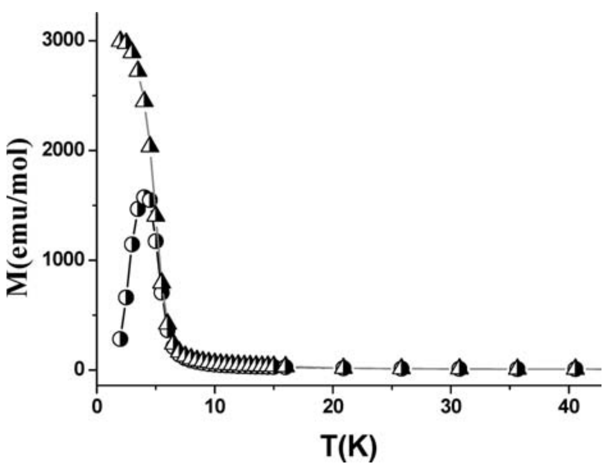

Figure 20. Thermal dependence of magnetization of **2**. Field-cooled (FC, triangles) and zero-field-cooled (ZFC, circles) magnetization at 100 Oe.

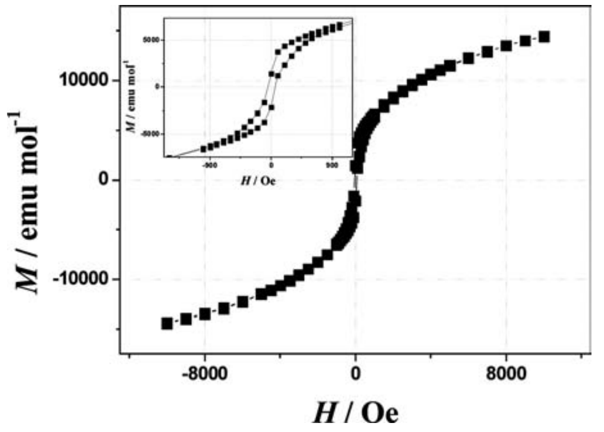

Figure 21. Field dependence of the magnetization of **2** at 5 K. The inset shows the hysteresis loop.

Figure 19 shows the temperature dependence of the molar susceptibility $\chi_M T(T)$ and $\chi^{-1}(T)$ of **2**. At room temperature, $\chi_M T$ is 3.79 cm^3 K mol^{-1} ($\mu_{eff} = 5.50\ \mu_B$), which is lower than the theoretical value for noncoupled high-spin (HS) Mn^{II} and low-spin (LS) Fe^{III} 4.75 cm^3 K mol^{-1} ($\mu_{eff} = 6.16\ \mu_B$) assuming $g = 2$. Upon cooling, $\chi_M T$ decreases slightly to the minimum value of 3.20 cm^3 K mol^{-} ($\mu_{eff} = 5.06\ \mu_B$) at 30 K and then abruptly increases to 97.75 cm^3 K mol^{-1} ($\mu_{eff} = 27.96\ \mu_B$) at 4 K and then rapidly decreases to 59.83 cm^3 K mol^{-1} ($\mu_{eff} = 21.86\ \mu_B$) at 2 K. The magnetic behavior shows that, above 30 K, the complex shows antiferromagnetic interaction between

---

(39) Pokhodyna, K. I.; Dokukin, V.; Miller, J. S. *Inorg. Chem.* **2008**, *47*, 2249–2251.

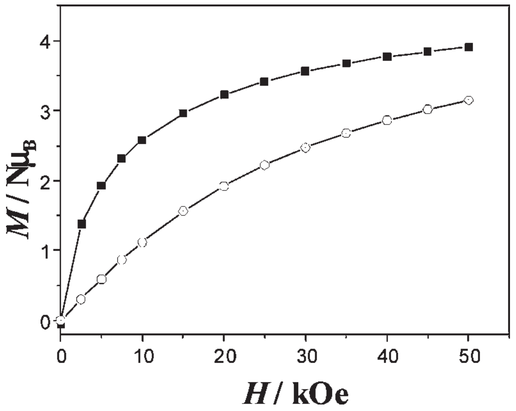

Figure 22. Magnetization as function of the applied field for **2** between 0 and 50 kOe at 5 K (black squares) and at 10 K (open circles).

the metal centers, whereas below 30 K, the metal ions {HS Mn(II) and LS Fe(III)} couple ferromagnetically. In accordance with this, the Currie–Weiss plots in the temperature ranges of 50–300 K and 5–18 K show a negative and a positive Weiss constant of $\theta = -9.7$ K and +4.8 K, respectively. This metamagnetic behavior[40] can be assigned to the combination of intralayer ferromagnetic and interlayer antiferromagnetic interactions, with the interlayer separations being less than 10 Å.

Figure 20 shows the temperature dependence of the zero-field-cooled (ZFC) and field-cooled (FC) magnetization, $M(T)_{\mathrm{ZFC}}$ and $M(T)_{\mathrm{FC}}$, respectively, of **2** under an applied field of 100 G. A magnetic ordering temperature of 4.5 K is observed, at which the field-cooled and the zero- field-cooled curves diverge. $M(T)_{\mathrm{ZFC}}$, after reaching a maximum at 4 K, gradually decreases, possibly due to domain wall freezing, as observed for $K_x\mathrm{Co[Fe(CN)_6]}_y\cdot 2H_2O$.[41] The $M(T)_{\mathrm{FC}}$ rises upon further cooling and has a bifurcation at 5 K, suggesting considerable irreversibility. The field dependence of the magnetization of **2** was measured in the field range of −10 000 to +10 000 Oe at 5 K (Figure 21). The curve is sigmoidal, and above 1000 Oe, it gradually increases without reaching the saturation value within the range of the measurement field. However, the curve shows a small hysteresis with a coercive field and a remnant magnetization value of 47 Oe and 0.26 $N\mu_{\mathrm{ss}}$, respectively. This is indicative of some ferromagnetic interaction.

In order to confirm the metamagnetic transition, the magnetization was determined as a function of the external magnetic field at 5 and 10 K (Figure 22). As was observed at lower field strengths, the dependence at 5 K shows a rapid increase below 250 G and then increases gradually at higher fields to approach a saturation value of 3.9 $N\mu_{\mathrm{B}}$ at 50 KOe, which is an indication of a phase transition to a ferromagnetic state. This phase transition is not observed at 10 K. Overall, however, it is important to note that although the data support assignment of the material as being metamagnetic, it is also possible that the phenomena observed are due to spin glass behavior.

The temperature-dependent molar magnetic susceptibility, χ_{M}, of the single crystal of **3** between 5 and 300 K is shown as $\chi_{\mathrm{M}}T(T)$ and $\chi^{-1}(T)$ in Figure 23. $\chi_{\mathrm{M}}T$ at room temperature is 0.375 cm^3 K mol^{-1} ($\mu_{\mathrm{eff}} = 1.73\,\mu_{\mathrm{B}}$), which is similar to that obtained for the $\mathrm{(Ph_4P)_2[Fe^{III}(CN)_5\text{-}imidazole]\cdot 2H_2O}$ and is expected for a low-spin iron(III) compound with regard to the diamagnetic nature of Zn(II). The $\chi^{-1}(T)$ curve is linear and intercepts the axis almost through zero, indicative of a paramagnetic compound. As the temperature is lowered, the value of $\chi_{\mathrm{M}}T$ remains constant until 45 K, then steadily decreases to 0.320 cm^3 K mol^{-1} ($\mu_{\mathrm{eff}} = 1.6\,\mu_{\mathrm{B}}$) at 5 K, which indicates weak intramolecular antiferromagnetic (AF) coupling between isolated low-spin iron(III) centers through the −CN−Zn−NC− bonding system; the $\mathrm{Fe^{III}\cdots Fe^{III}}$ distance in the structure of **3** is 9.943 Å.

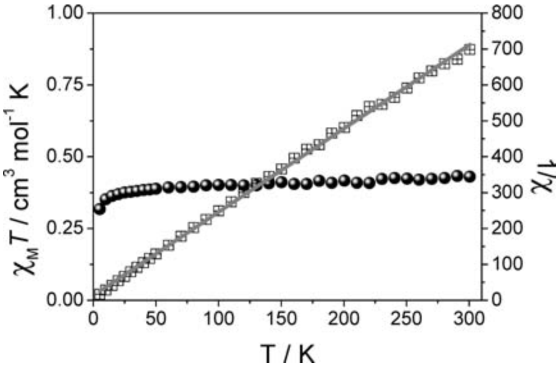

Figure 23. Temperature dependence of $\chi_{\mathrm{M}}T$ (circles) and $1/\chi_{\mathrm{M}}$ (squares) for **3**. The solid line represents the Currie–Weiss law plot at 100 G.

The plot of $\chi_{\mathrm{M}}T(T)$ for **4** is shown in Figure 24. The $\chi_{\mathrm{M}}T$ value (4.06 cm^3 K mol^{-1}, 5.70 μ_{B}) at 300 K is lower than the expected value 4.75 cm^3 K mol^{-1} ($\mu_{\mathrm{eff}} = 6.16\,\mu_{\mathrm{B}}$; calculated assuming $g = 2$) for the noncoupled HS $\mathrm{Mn^{II}}$ ($S = 5/2$) and LS $\mathrm{Fe^{III}}$ ($S = 1/2$). The slightly lower value of $\chi_{\mathrm{M}}T$ than that calculated indicates that the solid sample used for the magnetic measurement contains dinuclear species of the form HS $\mathrm{Mn^{III}}$ ($S = 2$)/LS $\mathrm{Fe^{II}}$ ($S = 0$). With decreasing temperature, $\chi_{\mathrm{M}}T$ decreases smoothly to a minimum value of 3.22 cm^3 K mol^{-1} ($\mu_{\mathrm{eff}} = 5.075\,\mu_{\mathrm{B}}$) at 15 K, then sharply increases to reach a maximum of 15.76 cm^3 K mol^{-1} ($\mu_{\mathrm{eff}} = 11.23\,\mu_{\mathrm{B}}$) at 3.5 K, and rapidly decreases to 5.88 cm^3 K mol^{-1} ($\mu_{\mathrm{eff}} = 6.86\,\mu_{\mathrm{B}}$) at 2 K, indicative of short-range antiferromagnetic interaction. This is confirmed by the $\chi^{-1}(T)$ value, in which the plot above 20 K obeys the Currie–Weiss law (Figure 24) showing a negative Weiss constant of $\theta = -6.5$ K. The highly distorted structure precludes alignment of the spins of the metal centers.

Conclusions

We have described a series of new bimetallic materials based on the $\mathrm{[Fe^{III}(CN)_5imidazole]^{2-}}$ building block. The single crystal of a paramagnetic 3D network for $\mathrm{Zn^{II}/Fe^{III}}$ was obtained with the $\mathrm{Zn^{II}}$ ions pentacoordinated to cyano ligands through nitrogen and forming a square pyramidal structure around the zinc ions. By contrast, the $\mathrm{Co^{II}/Fe^{III}}$ and $\mathrm{Mn^{II}/Fe^{III}}$ systems crystallize as 2D networks. The preference of the latter bimetallic complexes to crystallize in a 2D network is ascribed to the effect of the nonbridging imidazole ligand, the π acceptor[42] ability of which results in a trans effect, reducing the σ-donor strength of the axial cyano

---

(40) Re, N.; Crescenzi, R.; Floriani, C.; Miyasaka, H.; Matsumoto, N. *Inorg. Chem.* **1998**, *37*, 2717–2722.

(41) Kumar, A.; Yusuf, S. M. *Physica B* **2005**, *362*, 278.

(42) Johnson, C. R.; Shepherd, R. E.; Marr, B.; O'Donnell, S.; Dressick, W. *J. Am. Chem. Soc.* **1980**, *102*, 6227.

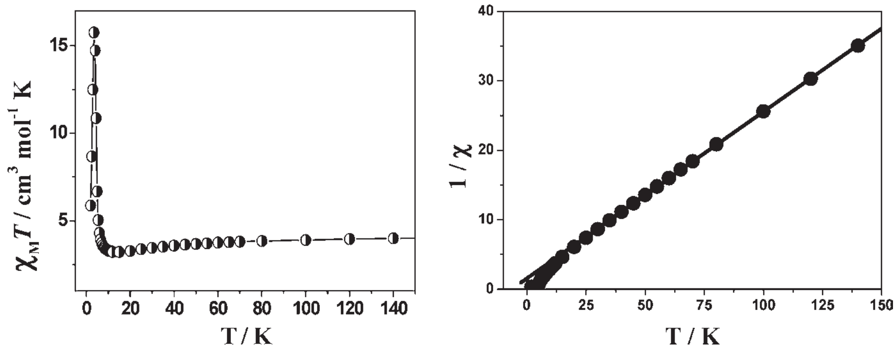

Figure 24. Temperature dependence of $\chi_M T$ (left) and $1/\chi_M$ (right) for **4**. The solid line represents the Currie−Weiss law plot.

ligand. The layers are made up of deformed square grids from tetrameric $[-M^{II}-CN-Fe^{III}-]_2$ (M = Mn or Co) units. The metal centers are in an octahedral geometry with the counter metal ion, forming four equatorial bonds with the equatorial cyano ligands through nitrogen atoms, and bind two solvent molecules in a *trans* fashion (water in the case of **1** and methanol in the case of **2**). The coordination of the imidazole to the iron ion results in a significant *trans* effect on the axial cyanide ligand, which reduces its ability to bridge a second metal ion. The magnetic studies carried out on these compounds reveal ferromagnetic behavior for **1** and **2** and a weak antiferromagnetic property for the Mn^{II}/Fe^{III} system **4**. The deviation of the layer structure from planarity (less pronounced for **1**) induces non-colinearity of the metal centers and hence spins, enhancing the disorder of spins and thereby increasing the paramagnetic character of the materials formed. In this study, we demonstrate that the building block $[Fe(III)(CN)_5(imidazole)]^{2-}$ is a versatile component in the preparation of new materials exhibiting a diverse range of magnetic properties. Furthermore, it shows that the imidazole ligand, while not forming a bridge between metal centers itself, has a profound influence on the bridging ability of the CN^- ligands. In principle, the use of substituted imidazoles offers a considerable handle on tuning the solid state properties. However, it should be noted that the synthetic route used to make the building block does not allow for this. Nevertheless, the preparation of the Mn(bpy)-based bimetallic material does indicate that further tuning of, for example, the properties of **4** is a worthwhile direction in which to proceed in obtaining new materials in this class.

Acknowledgment. The authors thank the Ubbo Emmius Scholarship (HT) and The Netherlands Organization for Scientific Research (NWO) for a Vidi grant (W.R.B.) and Mr. Jacob Baas for assistance with the magnetic measurements.

Supporting Information Available: Selected bond lengths and angles for **1**−**4**. This material is available free of charge via the Internet at http://pubs.acs.org.